0026-895X/00/061502-09$3.00/0
MOLECULAR PHARMACOLOGY
Copyright © 2000 The American Society for Pharmacology and Experimental Therapeutics
Mol Pharmacol 58:1502–1510, 2000

Vol. 58, No. 6
398/868462
Printed in U.S.A.

Competitive Antagonism of Recombinant $P2X_{2/3}$ Receptors by 2′,3′-*O*-(2,4,6-Trinitrophenyl) Adenosine 5′-Triphosphate (TNP-ATP)

EDWARD C. BURGARD, WENDE NIFORATOS, TIM VAN BIESEN, KEVIN J. LYNCH, KAREN L. KAGE, EDWARD TOUMA, ELIZABETH A. KOWALUK, and MICHAEL F. JARVIS

Neurological and Urological Diseases Research, Pharmaceutical Products Division, Abbott Laboratories, Abbott Park, Illinois

Received July 6, 2000; accepted September 12, 2000

This paper is available online at http://www.molpharm.org

ABSTRACT

TNP-ATP has become widely recognized as a potent and selective P2X receptor antagonist, and is currently being used to discriminate between subtypes of P2X receptors in a variety of tissues. We have investigated the ability of TNP-ATP to inhibit α,β-methylene ATP (α,β-meATP)-evoked responses in 1321N1 human astrocytoma cells expressing recombinant rat or human $P2X_{2/3}$ receptors. Pharmacological responses were measured using electrophysiological and calcium imaging techniques. TNP-ATP was a potent inhibitor of $P2X_{2/3}$ receptors, blocking both rat and human receptors with IC_{50} values of 3 to 6 nM. In competition studies, 10 to 1000 μM α,β-meATP was able to overcome TNP-ATP inhibition. Schild analysis revealed that TNP-ATP was a competitive antagonist with pA_2 values of −8.7 and −8.2. Inhibition of $P2X_{2/3}$ receptors by TNP-ATP was rapid in onset, reversible, and did not display use dependence. Although the onset kinetics of inhibition were concentration-dependent, the TNP-ATP off-kinetics were concentration-independent and relatively slow. Full recovery from TNP-ATP inhibition did not occur until ≥5 s after removal of the antagonist. Because of the slow off-kinetics of TNP-ATP, full competition with α,β-meATP for receptor occupancy could be seen only after both ligands had reached a steady-state condition. It is proposed that the slowly desensitizing $P2X_{2/3}$ receptor allowed this competitive interaction to be observed over time, whereas the rapid desensitization of other P2X receptors ($P2X_3$) may mask the detection of competitive inhibition by TNP-ATP.

P2X receptors comprise a family of seven distinct gene products that encode ATP-gated ion channel subunits ($P2X_{1-7}$, Ralevic and Burnstock, 1998). The protein subunits combine as either homomultimers (i.e., $P2X_3$) or heteromultimers (i.e., $P2X_{2/3}$) to form functional membrane-spanning multimeric receptors. Inclusion of multiple subunits into a functional receptor can confer a distinct biophysical as well as pharmacological identity to a particular receptor subtype (Lewis et al., 1995; Torres et al., 1998). For example, the ATP analog, α,β-methylene ATP (α,β-meATP), displays a nanomolar EC_{50} value for activation of the rapidly desensitizing rat $P2X_3$ homomultimeric receptor, whereas the EC_{50} value for activation of the nondesensitizing $P2X_{2/3}$ receptor is in the micromolar range (Bianchi et al., 1999). Although the exact stoichiometry of P2X receptors is not known, there is some evidence that they may exist as trimers or multiples of these (Nicke et al., 1998; Ding and Sachs, 1999; Stoop et al., 1999).

Historically, pharmacological investigation of P2X receptors has been hampered by the lack of potent, subtype-selective ligands. Antagonists such as suramin, pyridoxal-5-phosphate-6-azophenyl-2′,4′-disulfonic acid, reactive blue 2, and their analogs have traditionally been used as P2X receptor antagonists (Connolly, 1995; Bultmann et al., 1996). However, these compounds are relatively nonselective and exhibit high nanomolar-to-high micromolar affinities for P2X receptors (Bianchi et al., 1999). The ATP analog 2′,3′-*O*-(2,4,6-trinitrophenyl) adenosine 5′-triphosphate (TNP-ATP) has been used as a probe for more than two decades to label ATP-binding sites on a variety of tissues (Hiratsuka and Uchida, 1973; Watanabe and Inesi, 1982; Mockett et al., 1994). Mockett et al. (1994) and King et al. (1997) were among the first to describe the antagonist effects of TNP-ATP at P2X receptors. However, it was not until recently that Virginio et al. (1998) described the selective antagonism of $P2X_1$, $P2X_3$, and $P2X_{2/3}$ receptors by low nanomolar concentrations of TNP-ATP. This potent and relatively selective P2X receptor antagonist has now been used to characterize a variety of native P2X receptors (Lewis et al., 1998; Thomas et al., 1998; Burgard et al., 1999; Grubb and Evans, 1999; Zhong et al., 2000).

TNP-ATP is a close structural analog of ATP, suggesting that it may bind in the extracellular ATP binding pocket on P2X receptors, and may act as a competitive antagonist. This appeared to be the case when nondesensitizing ATP responses on cochlear hair cells were blocked by TNP-ATP in a competitive manner (Mockett et al., 1994). However, a more

ABBREVIATIONS: α,β-meATP, α,β-methylene ATP; TNP-ATP, 2′,3′-*O*-(2,4,6-trinitrophenyl) adenosine 5′-triphosphate.

recent characterization (Virginio et al., 1998) contained strong evidence that TNP-ATP was a noncompetitive antagonist of rapidly desensitizing recombinant $rP2X_3$ receptors. The apparent discrepancy between competitive and noncompetitive inhibition by an antagonist at receptor subtypes with different desensitization kinetics has been previously investigated using nicotinic receptor subtypes (Alkondon et al., 1992; Briggs and McKenna, 1996). These studies indicated that rapid receptor desensitization kinetics can make a competitive antagonist appear to be noncompetitive in functional assays.

We have re-examined the antagonist profile of TNP-ATP and have determined that it is a competitive antagonist of nondesensitizing $rP2X_{2/3}$ receptors. Here we show that, because of the slow off-kinetics of TNP-ATP at P2X receptors, competition between agonist and antagonist can best be measured using nondesensitizing $P2X_{2/3}$ receptors. TNP-ATP appears to be a noncompetitive antagonist at $rP2X_3$ receptors, but we propose that the rapid desensitization of $rP2X_3$ receptors prevents a competitive interaction from being measured. Preliminary results from these studies have been presented in abstract form (Niforatos et al., 1999).

Materials and Methods

Cell Culture. Stably transfected 1321N1 human astrocytoma cells expressing either rat $P2X_{2/3}$ ($rP2X_{2/3}$) or human $P2X_{2a/3}$ ($hP2X_{2a/3}$) receptors have previously been described (Bianchi et al., 1999; Burgard et al., 1999; Lynch et al., 1999). Briefly, these heteromultimeric cell lines were constructed by transfecting $rP2X_2$ or $hP2X_{2a}$ cDNA into stably transfected rat or human $P2X_3$-expressing cells using standard lipid-mediated transfection methods. Cell lines were maintained in Dulbecco's modified Eagle's medium containing 10% fetal bovine serum and antibiotics as follows: $hP2X_3$, 300 μg ml^{-1} G418; $hP2X_{2a}$, 100 μg ml^{-1} hygromycin; and $hP2X_{2a/3}$, 150 μg ml^{-1} G418 and 75 μg ml^{-1} hygromycin.

Electrophysiology. Patch-clamp recordings were performed as described previously (Burgard et al., 1999). Briefly, 1321N1 cells expressing $rP2X_{2/3}$ receptors were plated on polyethylenimine-coated coverslips and grown to approximately 50% confluence. Whole-cell patch-clamp recordings were obtained using a modified extracellular saline consisting of 155 mM NaCl, 5 mM KCl, 2 mM $CaCl_2$, 1 mM $MgCl_2$, 10 mM HEPES, and 12 mM glucose. The intracellular patch pipette solution consisted of 140 mM potassium aspartate, 20 mM NaCl, 10 mM EGTA, and 5 mM HEPES. All cells were voltage-clamped at −60 mV, and series resistance compensated 85 to 90% using an Axopatch 200B amplifier (Axon Instruments, Foster City, CA).

Drugs were applied to the cells using a piezoelectric-driven glass theta tube positioned near the cell. The solution interface between barrels was swept across the cell. Solution exchange times were often recorded by application of a 90% extracellular saline (10% water added) across an open pipette tip. A single exponential function was fitted to the resulting junction current transient, giving an open-tip response time constant (τ). Alternatively, whole-cell exchange τs were recorded in whole-cell patch mode by application of α,β-meATP (10 μM) to activate $rP2X_{2/3}$ receptors, and switching into and out of a high (55 mM) potassium-containing solution. The resulting potassium-generated current relaxation through open P2X receptors gave an indication of the whole-cell exchange time. During experiments, agonists were usually applied every 30 to 60 s. Agonist applications were kept short (most <3 s) to minimize pore dilation of $P2X_{2/3}$ receptors (Khakh et al., 1999). No evidence of pore dilation was observed.

Responses were acquired and digitized at 3 kHz, and analyzed using pClamp software (Axon Instruments). Current amplitudes were always measured at the end of the agonist application pulse. Current on- and off-responses were fitted with a single exponential function, and the resulting τs were calculated. Agonist concentration-response curves were fitted by least-squares regression to the logistic equation:

$$Y = \min + [(\max - \min)/(1 + 10^{(\mathrm{LogEC_{50}} - X)n_H})]$$

where Y, min, and max represent the measured, minimum, and maximum responses, respectively; EC_{50} is the ligand concentration giving half-maximal response; X is the concentration of ligand used; and n_H is the Hill coefficient (Prism; GraphPad Software, San Diego, CA). Antagonist concentration-response curves were fitted in the same manner to determine IC_{50} values. The inhibition constant (K_i) for the competitive antagonist TNP-ATP was estimated from its IC_{50} value using the Cheng-Prusoff relationship (Cheng and Prusoff, 1973; Craig, 1993): $K_i = IC_{50} / (1 + A/EC_{50})$, where A represents the concentration of agonist, and EC_{50} represents the agonist EC_{50}.

Competitive inhibition was determined using Schild analysis (Arunlakshana and Schild, 1959). The log concentration ratio log (A′ / A − 1) was plotted against TNP-ATP concentration. A and A′ represent agonist EC_{50} values obtained in the absence and presence of TNP-ATP, respectively. pA_2 values were determined from least-squares linear regression fitted to the Schild plots. Throughout the text, data are expressed as mean ± S.E.M.

Calcium Imaging. Inhibition of $hP2X_{2a/3}$ or $rP2X_{2/3}$ receptors by TNP-ATP was also studied by measuring changes in cytosolic calcium levels. The fluorescent dye Fluo-4 was used as an indicator of the relative levels of intracellular calcium in a 96-well format using a fluorescence imaging plate reader (Molecular Devices, Sunnyvale, CA), as described previously (Bianchi et al., 1999). TNP-ATP (50 μl of 4× concentration) was added 3 min before the addition of α,β-meATP (50 μl of 4× concentration, final volume = 200 μl). Fluorescence intensities were measured at 1- to 5-s intervals throughout each experimental run. Data shown are based on the peak increase in relative fluorescence units compared with basal fluorescence. Concentration-response curves are shown as a percentage of the maximum α,β-meATP-mediated fluorescence signal measured in the absence of TNP-ATP.

All reagents were obtained from Sigma Chemical Co. (St. Louis, MO.) unless otherwise noted. TNP-ATP and Fluo-4 were purchased from Molecular Probes (Eugene, OR), and suramin from Research Biochemicals International (Natick, MA).

Results

Drug Application. The chemical structures of ATP and TNP-ATP are shown in Fig. 1A. For TNP-ATP, the nucleotide has been modified to include a trinitrophenyl group on the 2′,3′ dihydroxy position. The structural similarity of TNP-ATP to ATP suggested that both molecules may interact with the same binding site on the P2X receptor.

To determine the mechanism of action of TNP-ATP, a rapid application system was used to apply agonists and antagonists to 1321N1 cells expressing $rP2X_{2/3}$ receptors (under *Materials and Methods*). Solution exchange times were determined under a variety of conditions (Fig. 1B). Exchange of the solution interface across an open pipette tip was achieved in approximately 1 to 2 ms (1.6 ± 0.1 ms, n = 10). This provided an indication of how fast the solution interface could travel across a pipette. In contrast, whole-cell exchange time constants were 20.6 ± 0.3 ms (n = 5), indicating that diffusion around an entire cell was approximately 10 to 20 times slower than diffusion across an open pipette tip. Similar activation (32 ± 5.5 ms, Fig. 1B) and deactivation (86 ± 13 ms) time constants (τ) for 10 μM α,β-meATP-induced cur-

rents were also recorded (n = 20), indicating that activation and deactivation rates were close to being diffusion-limited. Because α,β-meATP exchange rates approached the limits of diffusion, no quantitative conclusions were drawn regarding the actual activation and deactivation rates of P2X receptors. However, comparisons were made to the slower rates of receptor antagonism by TNP-ATP (see below).

Competitive Inhibition by TNP-ATP. TNP-ATP inhibited $P2X_{2/3}$ receptors in a concentration-dependent manner as assayed either by patch-clamp (Fig. 2, A and B) or calcium imaging (Fig. 2B) techniques. As can be seen in Fig. 2A, activation of $P2X_{2/3}$ receptors by α,β-meATP resulted in a non- or very slowly desensitizing inward current. Because these receptors were relatively nondesensitizing, agonist could be applied and removed as frequently as every 15 s without a decrease in current amplitude. Concentration-dependent inhibition by TNP-ATP was evident from patch-clamp recordings both as an increase in the amount of inhibition (gradual decrease in current amplitude), as well as an increase in the rate at which inhibition developed. Both agonist and antagonist were coapplied in Fig. 2A, and the extent of inhibition was measured at the end of the application. Calculated IC_{50} values for TNP-ATP were obtained from inhibition curves for both $rP2X_{2/3}$ and $hP2X_{2a/3}$ receptors, using two different functional assays (Fig. 2B). For $rP2X_{2/3}$ receptors, patch-clamp recordings revealed an IC_{50} value of 5.5 ± 1.1 nM (n = 3–11 cells/concentration), and intracellular calcium responses revealed an IC_{50} value of 3.0 ± 1.1 nM (n = 5 experiments). For $hP2X_{2a/3}$ receptors, intracellular calcium responses revealed an IC_{50} value of 4.6 ± 1.2 nM (n = 3 experiments). It should be noted that in these series of experiments, the IC_{50} values for TNP-ATP were almost identical, even when measured at different receptors and under different assay conditions.

To evaluate the competitive nature of TNP-ATP antagonism, competition curves were constructed for TNP-ATP inhibition of $rP2X_{2/3}$ (electrophysiology, Fig. 3A) and $hP2X_{2a/3}$ (calcium imaging, Fig. 3B) receptors. As can be seen from both sets of graphs, increasing concentrations of α,β-meATP were able to fully overcome inhibition produced by TNP-ATP over a range of concentrations. A similar rightward shift of the α,β-meATP concentration-response curve was observed when calcium imaging experiments were performed using $rP2X_{2/3}$ receptors (data not shown). Schild analysis of both rat and human receptors (Fig. 3, A and B, insets) revealed plots best fitted with a regression line of slope 1.0 ($hP2X_{2a/3}$) or 1.1 ($rP2X_{2/3}$). pA_2 values obtained from Schild analysis were −8.2 (6 nM) for $hP2X_{2a/3}$ and −8.7 (2 nM) for $rP2X_{2/3}$. Parallel right-shifted competition curves with a Schild plot of slope = 1 were consistent with competitive antagonism of α,β-meATP with TNP-ATP at both human and rat $P2X_{2/3}$ receptors

Assuming competitive binding at the $P2X_{2/3}$ receptor, K_i values were calculated from TNP-ATP IC_{50} values using the Cheng-Prusoff relationship (under *Materials and Methods*). Agonist concentrations of 3 μM ($hP2X_{2a/3}$) and 10 μM ($rP2X_{2/3}$) α,β-meATP were used in these experiments. The EC_{50} values for α,β-meATP were 3.4 μM ($rP2X_{2/3}$, Bianchi et al., 1999) and 1.3 μM ($hP2X_{2a/3}$; H. McDonald and E. C. Burgard, unpublished observations), as determined from agonist concentration-response curves. Calculated K_i values for TNP-ATP were 1.4 nM for both $rP2X_{2/3}$ and $hP2X_{2a/3}$. This was very similar to IC_{50} as well as calculated pA_2 values, in that all were between 1 and 10 nM. The high affinity of TNP-ATP for $P2X_{2/3}$ receptors was independent of species or assay conditions.

In contrast, calcium imaging experiments performed using the $hP2X_3$ receptor (Fig. 3C) revealed TNP-ATP competition curves characterized by a decrease in the maximal agonist-induced current, with a rightward shift in the agonist EC_{50} value. The apparent inability of α,β-meATP to overcome TNP-ATP block is in agreement with a published report (Virginio et al., 1998) that describes TNP-ATP as a noncompetitive antagonist at desensitizing $P2X_3$ receptors. However, this apparent discrepancy could be explained by differences in desensitization rates between the two receptor subtypes (see below).

Kinetics of TNP-ATP Inhibition. If TNP-ATP and α,β-meATP compete for the same binding site at $P2X_{2/3}$ receptors, then analysis of a competitive interaction should be performed when both ligands have achieved steady-state binding. This assumes that both ligands have had a sufficient amount of time to bind to (or unbind from) the receptor. The agonist-induced activation and deactivation kinetics of $P2X_{2/3}$ receptors approached the experimental limits of solution diffusion (Fig. 1B), suggesting that 10 μM α,β-meATP

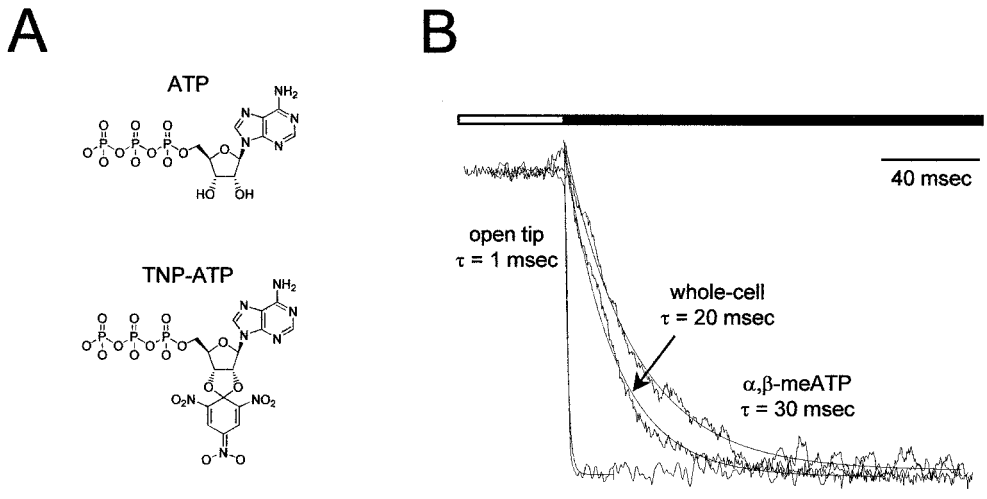

Fig. 1. Rapid agonist and antagonist application. A, chemical structures of the endogenous P2X receptor agonist ATP and the structural analog TNP-ATP are shown. B, solution exchange times were determined by whole-cell or pipette recording in control solution (open bar) and rapidly switching into test solution (closed bar, under *Materials and Methods*). A single exponential function was fitted to each response and the resulting time constant (τ) is shown. All currents have been scaled for visual comparison and the whole-cell current response has been inverted to maintain polarity. α,β-MeATP (10 μM) was used to activate $rP2X_{2/3}$ receptors.

probably reached steady-state binding in tens of milliseconds. However, it appeared that TNP-ATP on- and off-kinetics were much slower. To evaluate the on- and off-kinetics of TNP-ATP, three different drug application protocols were used in patch-clamp experiments to apply TNP-ATP to cells expressing $rP2X_{2/3}$ receptors (Fig. 4). TNP-ATP was either 1) preapplied, to measure the steady-state effects of TNP-ATP on subsequent activation by agonist; 2) postapplied, to measure both the on- and off-kinetics of TNP-ATP in the presence of agonist; or 3) coapplied, to measure TNP-ATP kinetics during simultaneous application with agonist.

The preapplication protocol is the conventional application method used to study antagonist potency and efficacy. Using this method, preapplication of TNP-ATP (≥30 s) allowed the antagonist to reach a steady-state interaction with the receptor before agonist was applied. As shown in Fig. 4, preapplication of TNP-ATP (100 nM) produced a decrease in both amplitude and apparent activation rate of the α,β-meATP (10 μM) response. This response resembled that of a low α,β-meATP concentration, and is consistent with the profile of a competitive interaction at the receptor. Because the α,β-meATP on-kinetics are fast, the slow activation seen in the presence of TNP-ATP is an indirect reflection of the slow off-kinetics of TNP-ATP (Benveniste et al., 1990; see below) because the competitive antagonist must unbind for agonist to activate the receptor. Here 100 nM TNP-ATP also inhibited the α,β-meATP-induced response to <10% of control, consistent with the concentration-response curve in Fig. 2B. In addition, the first agonist response was always inhibited after TNP-ATP application, so there was no evidence for a use-dependent mechanism of action of TNP-ATP. Although the preapplication method reveals the extent of steady-state inhibition by an antagonist, it provides only indirect information about the antagonist off-kinetics, and no information regarding the on-kinetics of antagonist interactions with the receptor.

To investigate the on- and off-kinetics of antagonists, the postapplication protocol was used because it allowed the antagonist kinetics to be measured entirely during steady-state receptor activation by agonist. As shown in Fig. 4, on- and off-response kinetics were recorded when $rP2X_{2/3}$ receptors were first activated by α,β-meATP (10 μM), and then TNP-ATP (100 nM) was applied and removed during steady-state receptor activation (postapplication). All on- and off-responses were adequately described by a single exponential function. Using this protocol, the 100 nM TNP-ATP on-response time constant τ_{on} was 320 ± 74 ms (n = 9), and the off-response time constant (τ_{off}) was 2390 ± 315 ms (n = 7). Even at this high IC_{90} concentration of TNP-ATP, it is evident that the on- and off-kinetics are ≥10-fold slower than 10 μM α,β-meATP kinetics. Antagonist steady state was reached after a sufficiently long TNP-ATP application, and the extent of inhibition was measured under these conditions. One minor drawback to this approach was the presence in some cells of very slow α,β-meATP-induced desensitization during "steady-state" agonist application. Agonist was often applied for >10 s before applying TNP-ATP, and the steady-state current amplitude decreased slightly in a proportion of cells. Although this did not affect either the TNP-ATP kinetics or extent of inhibition, it did shift the baseline amplitude

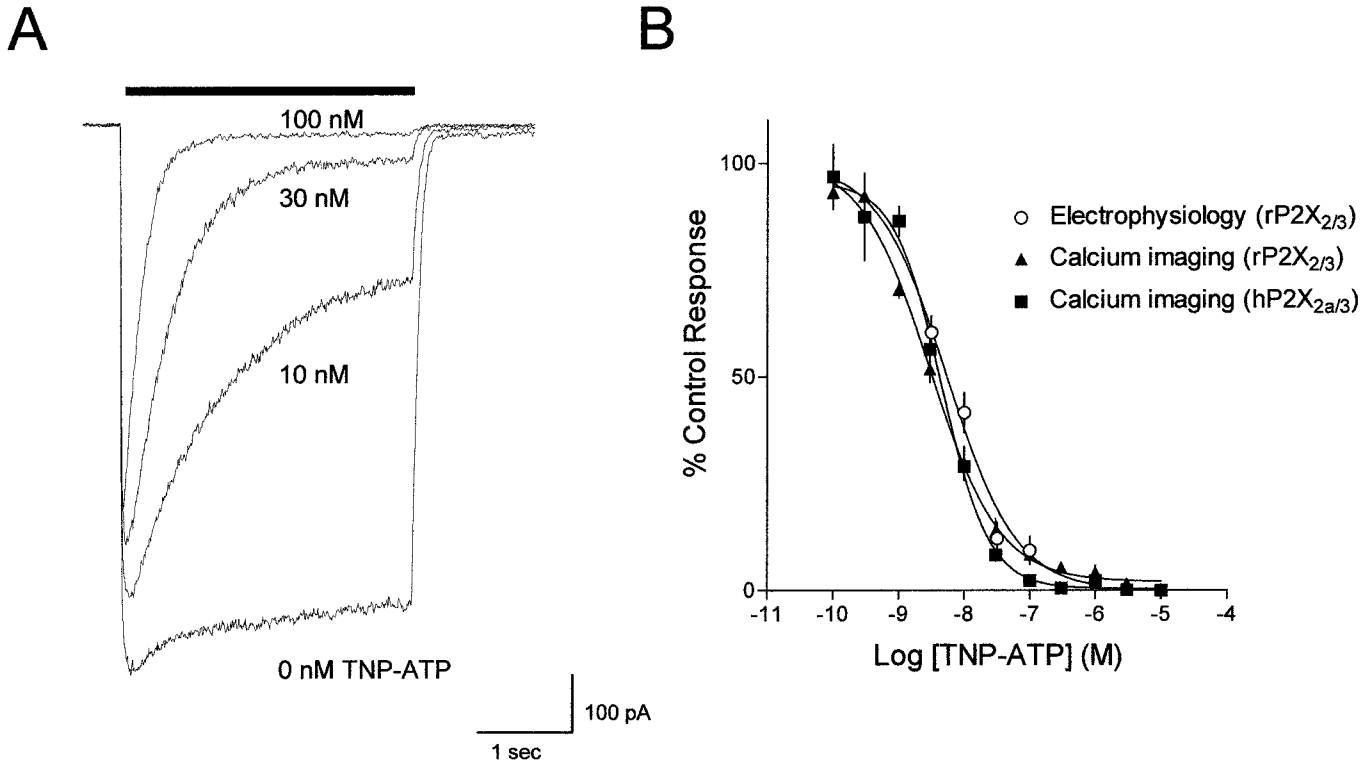

Fig. 2. Inhibition of $P2X_{2/3}$ responses by TNP-ATP. A, individual $rP2X_{2/3}$ currents recorded in response to 10 μM α,β-meATP (denoted by the bar). Increasing concentrations of TNP-ATP were coapplied (0–100 nM) with α,β-meATP and traces were superimposed. B, TNP-ATP concentration-response curves from two different $P2X_{2/3}$ receptors. Inhibition of 10 μM α,β-meATP responses by TNP-ATP at $rP2X_{2/3}$ receptors was measured using either patch-clamp recording (○) or calcium imaging (▲). TNP-ATP inhibition at $hP2X_{2a/3}$ receptors was measured using calcium imaging techniques (■). Data are expressed as percentage of a corresponding 10 μM ($rP2X_{2/3}$) or 3 μM ($hP2X_{2a/3}$) α,β-meATP response.

of the agonist response during TNP-ATP application. This effect can be seen in Fig. 4 (postapplication trace, asterisk).

Another approach used to study TNP-ATP kinetics was to apply both agonist and antagonist simultaneously, and then measure the effect of the antagonist under these conditions. This coapplication protocol eliminated any potential effects of slow agonist-induced desensitization on TNP-ATP kinetic measurements. When TNP-ATP was coapplied with α,β-meATP (Figs. 2 and 4, coapplication), currents activated rapidly, but a time-dependent inhibition of current developed (relatively slowly). Both the extent of block and the apparent rate at which inhibition occurred increased with increasing concentrations of TNP-ATP. Because agonist steady state was reached within the first 50 ms, it was assumed that antagonist on-kinetics could be reliably estimated if they were slower than 50 to 100 ms. Indeed, the α,β-meATP activation τ_{on} was the same whether applied alone (26 ± 10 ms, $n = 5$) or coapplied with 100 nM TNP-ATP (27 ± 12 ms, $n = 5$), indicating that TNP-ATP inhibition developed more slowly than α,β-meATP activation. As shown in Fig. 4, the 100 nM TNP-ATP τ_{on} for both coapplication (387 ± 91 ms, $n = 5$) and postapplication (320 ± 74 ms, $n = 9$) protocols was similar. Although the overall τ_{on} was slower at lower TNP-ATP concentrations (10 and 30 nM), these TNP-ATP τ_{on} were also not significantly different between co- and postapplication protocols. Because the TNP-ATP on-kinetics were slow, and a relatively long (≥2 s) application was used, a reasonable estimate of both τ_{on} and extent of inhibition was obtained using the coapplication protocol.

All three protocols resulted in similar τ_{on} and/or τ_{off} values for TNP-ATP. It is important to note that for concentrations of TNP-ATP ≤ IC_{90}, τ_{on} and τ_{off} kinetics were ≥10 times slower than α,β-meATP kinetics. At these concentrations, TNP-ATP inhibition developed slowly, and recovery from inhibition was correspondingly slow.

Of the three protocols, measurements using the postappli-

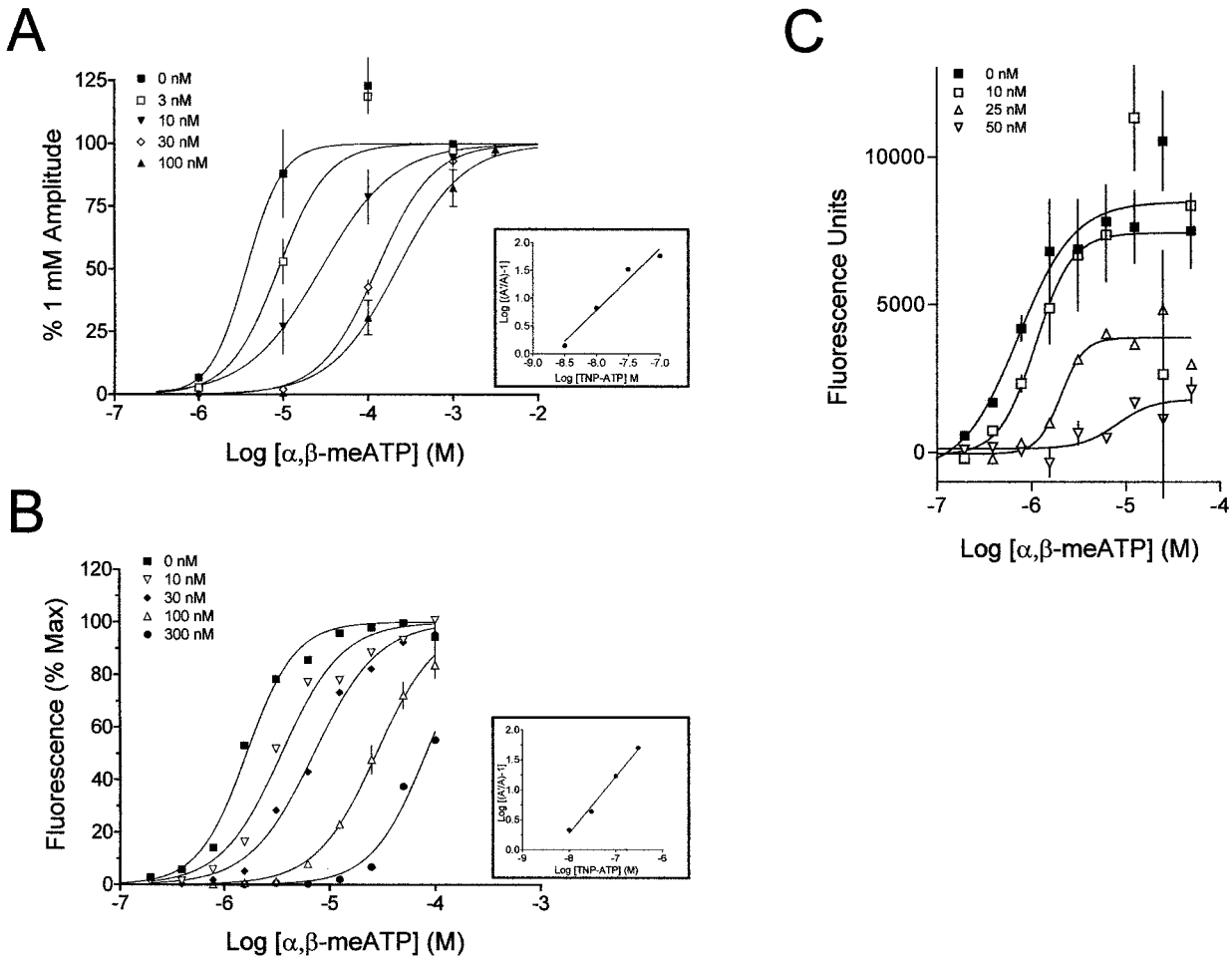

Fig. 3. Competitive inhibition by TNP-ATP at different $P2X_{2/3}$ receptors. A, concentration-response curves for α,β-meATP in the presence of increasing concentrations of TNP-ATP were measured using electrophysiological techniques on cells expressing the $rP2X_{2/3}$ receptor. Data (n = 3–14 cells/data point) are plotted as percentage of 1 mM α,β-meATP-induced current amplitude. Boxed inset, Schild plot of the data shown in A. B, concentration-response curves for α,β-meATP in the presence of increasing concentrations of TNP-ATP were measured using calcium imaging techniques on cells expressing the $hP2X_{2a/3}$ receptor. Data (n = 3 experiments/data point) are plotted as percentage of maximal α,β-meATP-induced Fluo-4 fluorescence. A maximal concentration of 100 μM α,β-meATP was used for these experiments. Boxed inset, Schild plot of the data shown in B. For A and B, upper and lower limits of curves were constrained to 100 and 0% of response, respectively. For Schild plots, concentration ratios were calculated and plotted as detailed under *Materials and Methods*. pA2 values were determined from the x-intercept of a regression line fitted to the data. C, concentration-response curves for α,β-meATP in the presence of increasing concentrations of TNP-ATP were measured using calcium imaging techniques on cells expressing the $hP2X_3$ receptor. Data (n = 2 experiments/data point) are plotted as α,β-meATP-induced Fluo-4 fluorescence units as recorded in the assay. For A to C, TNP-ATP concentrations and their corresponding symbols are displayed in the upper left corner of each graph.

cation method best represented the true on- and off-kinetics of TNP-ATP inhibition. Using this protocol, the concentration dependence of τ_{on} and τ_{off} was further investigated. As shown in Fig. 5A, the τ_{on} decreased with increasing concentrations of TNP-ATP. This concentration-dependent increase in the apparent rate of inhibition was consistent with a mass action increase in binding probability. However, the τ_{off} did not change with increasing TNP-ATP concentrations, indicating that the off-response kinetics were concentration-independent. The on- and off-kinetics of the P2X receptor antagonist suramin are shown in Fig. 5B. In comparison, suramin exhibits an IC_{50} value of approximately 800 nM at rat $P2X_{2/3}$ receptors (Bianchi et al., 1999). In this cell at equimolar concentrations (10 μM), suramin displayed much faster off-kinetics (τ_{off} = 775 ms) than TNP-ATP (τ_{off} = 5951 ms), consistent with its lower affinity for the $P2X_{2/3}$ receptor. A summary of the effects of TNP-ATP concentration on τ_{on} and τ_{off} from 15 cells is shown in Fig. 6. At all concentrations of TNP-ATP, the mean τ_{off} values were very slow (>2000 ms). It is reasonable to assume that the high affinity of TNP-ATP for $rP2X_{2/3}$ receptors is predominantly determined by its slow τ_{off}.

In contrast to $rP2X_{2/3}$ receptors, $rP2X_3$ receptors exhibit rapid desensitization in the presence of agonist (Lewis et al., 1995). The relationship between receptor desensitization and TNP-ATP time course can be seen in the traces in Fig. 7. Here α,β-meATP induced a nondesensitizing inward current at $rP2X_{2/3}$ receptors (α,β-meATP control trace). Preapplication of TNP-ATP (α,β-meATP + TNP-ATP trace) produced a decrease in the α,β-meATP activation rate due to competition of α,β-meATP with TNP-ATP. The slow τ_{off} of TNP-ATP is evident here because it takes >2 s to approach a steady-state interaction between agonist and antagonist. Only after this time can a competitive interaction be observed where agonist can replace the slowly dissociating antagonist at the receptor. The relatively nondesensitizing $rP2X_{2/3}$ receptor remains open long enough to detect the competition. In contrast, the rapid desensitization of $rP2X_3$ (light $P2X_3$ trace) receptors occurs before TNP-ATP can dissociate from the $rP2X_{2/3}$ receptor, precluding a steady-state competition to be recorded. Apparent noncompetitive inhibition would be observed at rapidly desensitizing $P2X_3$ receptors, due to the inability of TNP-ATP to dissociate before the current desensitized.

Discussion

TNP-ATP is a trinitrophenyl analog of ATP that binds to a variety of ATP-binding sites. When used as a fluorescent probe, relatively high concentrations have been used to label ATP-binding sites and to probe enzyme activities (Hiratsuka and Uchida, 1973; Watanabe and Inesi, 1982; Mockett et al., 1994). However, the nanomolar affinity of TNP-ATP for $P2X_1$, $P2X_3$, and $P2X_{2/3}$ receptors (Virginio et al., 1998) suggests that TNP-ATP may be a selective antagonist for these P2X receptors over other ATP-binding sites. Using these criteria, TNP-ATP is currently the most potent and selective P2X receptor antagonist available.

In the present study, we have confirmed the high affinity of TNP-ATP for $P2X_{2/3}$ receptors. Potent antagonism (IC_{50} < 10 nM) of both human and rat $P2X_{2/3}$ receptors by TNP-ATP was demonstrated using calcium imaging as well as electrophysiological techniques. TNP-ATP was determined to be a competitive antagonist based on a number of experimental results. First, the inhibition could be overcome by increasing concentrations of agonist. Second, parallel right-shifted agonist concentration-response curves were constructed in the presence of increasing concentrations of TNP-ATP, with no change in the maximal agonist response. Third, Schild analysis revealed a competitive inhibition by TNP-ATP at $P2X_{2/3}$ receptors. Fourth, calculated pA_2 values were also <10 nM, and correlated well with the IC_{50} value and calculated K_i values. A similar competitive antagonism of nondesensitizing

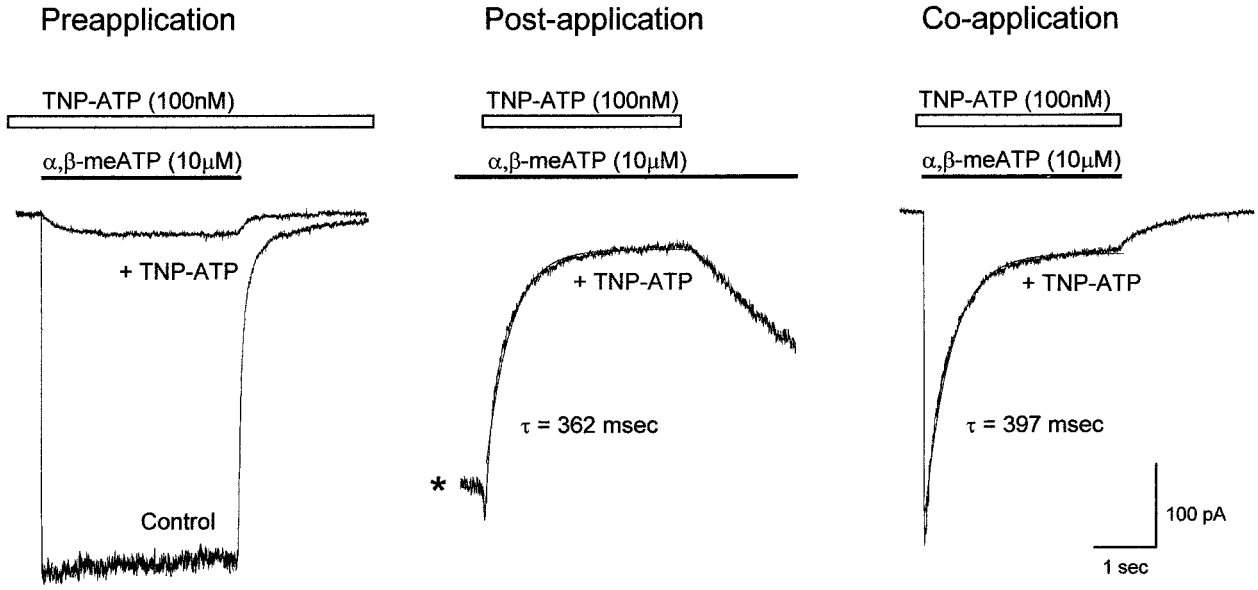

Fig. 4. Inhibition and kinetics of TNP-ATP are similar regardless of application protocol. TNP-ATP was applied with α,β-meATP using three different protocols in a single cell expressing $rP2X_{2/3}$ receptors. The control response to 10 μM α,β-meATP is shown along with the preapplication protocol trace. For preapplication, TNP-ATP (open bar) was applied at least 30 s before, during, and after α,β-meATP (solid bar) application. For postapplication, α,β-meATP was applied for 5 to 10 s before, during, and after TNP-ATP application. The asterisk denotes a baseline shift due to slow agonist-induced desensitization of the response. For coapplication, TNP-ATP and α,β-meATP were applied and removed at the same time. The τ_{on} of single exponential functions fitted to the TNP-ATP traces for post- and coapplication are shown.

P2X responses in cochlear hair cells was reported by Mockett et al. (1994), although the TNP-ATP concentrations used were orders of magnitude higher than those used in the present study. This was presumably due to lower affinity interactions of TNP-ATP with nondesensitizing cochlear $P2X_2$ receptors (Housley et al., 1999). From these two studies, it appears that TNP-ATP is a competitive antagonist of nondesensitizing P2X receptors.

In addition to confirming the high affinity of TNP-ATP for the $P2X_{2/3}$ receptor, we have demonstrated that the off-kinetics of TNP-ATP are very slow (>2000 ms), and is concentration-independent. It is proposed that the slow off-kinetics contribute to the high affinity of the antagonist, as well as contribute to its apparent noncompetitive action at $P2X_3$ receptors. However, to draw conclusions based on apparent antagonist kinetics, a number of experimental assumptions must be met. In relation to the kinetics of a competitive antagonist, the solution exchange rate, the binding and unbinding kinetics of the agonist, and the channel gating kinetics must all be fast (Benveniste et al., 1990; Benveniste and Mayer, 1991). In addition, the channel must be relatively nondesensitizing. Under these assumptions, agonist will reach equilibrium quickly, and the slow kinetics of the antagonist will be measurable. In the present studies, the on- and off-kinetics of 10 μM α,β-meATP approached the limits of whole-cell diffusion for our drug delivery system (τ = 20–30 ms). In comparison, the on-kinetics for TNP-ATP at an IC_{90} concentration was 10-fold slower, and the corresponding off-kinetics were >25-fold slower than the agonist. Although channel-gating kinetics have not been described adequately for either $P2X_3$ or $P2X_{2/3}$ receptors, channel opening and closing rates estimated from either recombinant or native P2X receptors indicate that these parameters are also significantly faster than TNP-ATP kinetics (Krishtal et al., 1988; Bean et al., 1990; Cloues, 1995; Wright and Li, 1995; Evans, 1996; Ding and Sachs, 1999). Having met these assumptions, the TNP-ATP kinetics measured in the present studies are a reasonable measure of apparent antagonist binding and unbinding rates.

Preapplication of a competitive antagonist for a sufficient period of time allows equilibrium to be reached between antagonist and receptor. Subsequent application of a rapidly

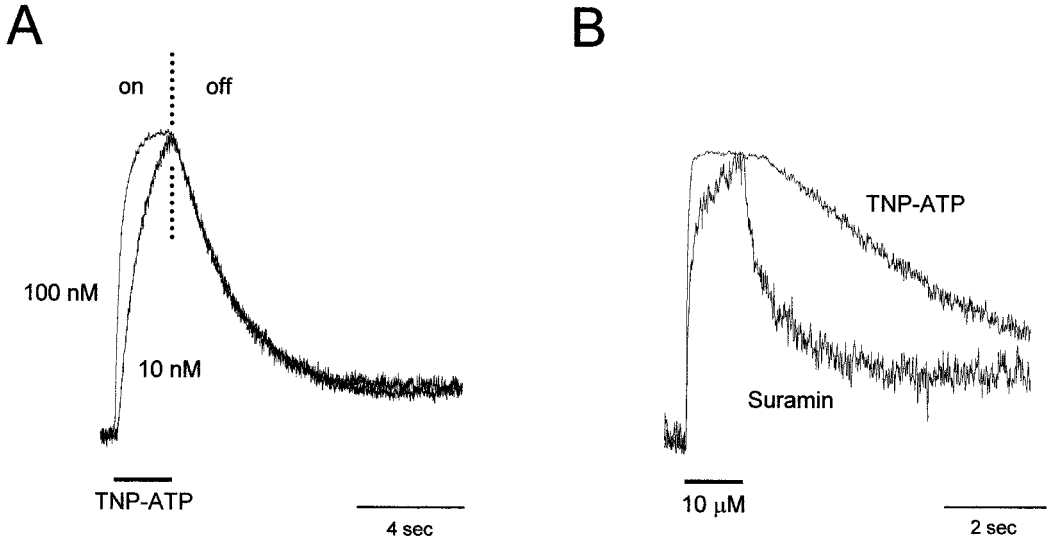

Fig. 5. Concentration-dependent kinetics of TNP-ATP. A, postapplication responses of TNP-ATP. α,β-meATP (10 μM) was applied before, during, and after TNP-ATP applications of 10 and 100 nM. Note the concentration dependence of TNP-ATP on-response only. Individual traces recorded from the same cell. B, equimolar concentrations (10 μM) of TNP-ATP or suramin show difference in kinetics. Both antagonists were applied to the same cell using the postapplication protocol. Note the faster on- and slower off-kinetics of TNP-ATP. For A and B, traces have been scaled to equal amplitudes for visual comparison.

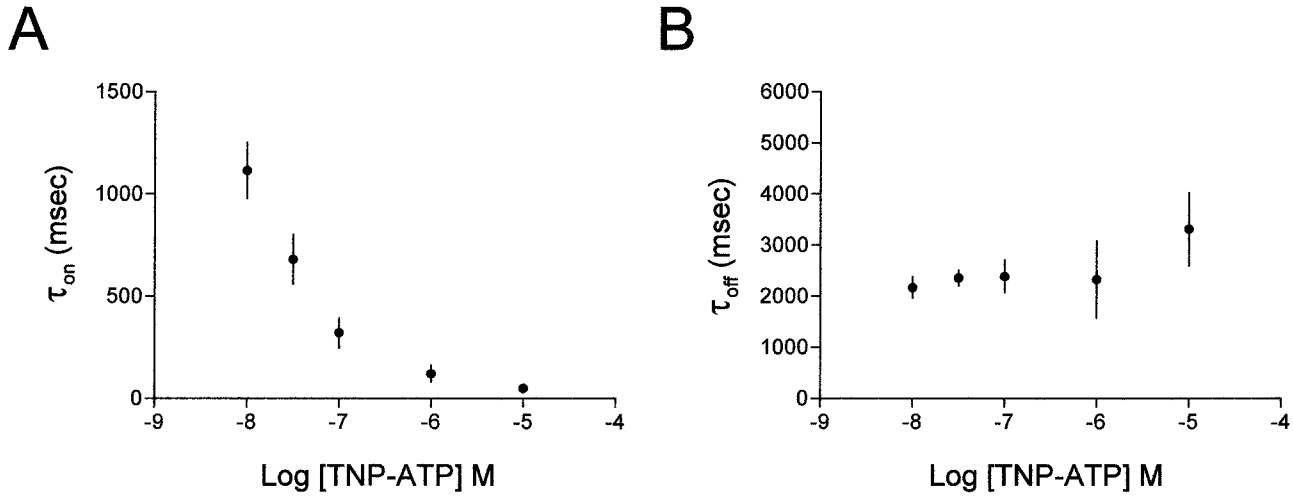

Fig. 6. Summary of TNP-ATP on- and off-kinetics. A, τ_{on} of TNP-ATP inhibition is concentration-dependent (n = 4–11 cells/data point). B, τ_{off} of TNP-ATP inhibition is not concentration-dependent (n = 3–10 cells/data point). For A and B, τs were determined from single exponential curves fitted to the TNP-ATP on- or off-response as in Fig. 5.

equilibrating agonist will result in a slow increase in agonist-activated current, reflecting the dissociation kinetics of the antagonist (Benveniste et al., 1990). Preapplication of TNP-ATP significantly slowed the subsequent agonist response and decreased its amplitude. This protocol gave a reliable measure of magnitude of inhibition by TNP-ATP, and allowed an indirect estimate of the off-kinetics of TNP-ATP. A better measure of TNP-ATP on- and off-kinetics was obtained by using the postapplication protocol, where agonist equilibrium was achieved first, and TNP-ATP was subsequently applied. The antagonist on-kinetics reflected the *apparent* on-rate because these kinetics depend on antagonist concentration, the intrinsic antagonist association and dissociation rates, and the concentration of agonist (Benveniste and Mayer, 1991). On the other hand, the measured TNP-ATP off-kinetics revealed a closer estimate to the true dissociation rate because these were concentration-independent and were sufficiently slow to not be influenced by rapid association and dissociation of agonist. Interestingly, we also found that if TNP-ATP was coapplied with agonist, the response reached a rapid peak, but a progressive decrease in agonist-activated current occurred with a kinetic profile that was similar to the on-kinetics measured using the postapplication protocol. It appeared that coapplication was a rapid way to obtain an estimate of the on-kinetics of TNP-ATP.

TNP-ATP was originally characterized as a potent, noncompetitive antagonist at rapidly desensitizing rat $P2X_3$ receptors (Virginio et al., 1998). Likewise, we have observed an apparent noncompetitive block by TNP-ATP at $rP2X_3$ receptors (Fig. 3C). This apparent competitive ($rP2X_{2/3}$) versus noncompetitive ($rP2X_3$) discrepancy between two receptor subtypes could be explained by intrinsic differences in the receptor desensitization rates. For example, a competitive antagonist of nondesensitizing nicotinic acetylcholine receptors appeared to be noncompetitive at rapidly desensitizing receptor subtypes (Alkondon et al., 1992; Briggs and McKenna, 1996). This effect was also due to rapid receptor desensitization occurring before slow dissociation of the high-affinity antagonist.

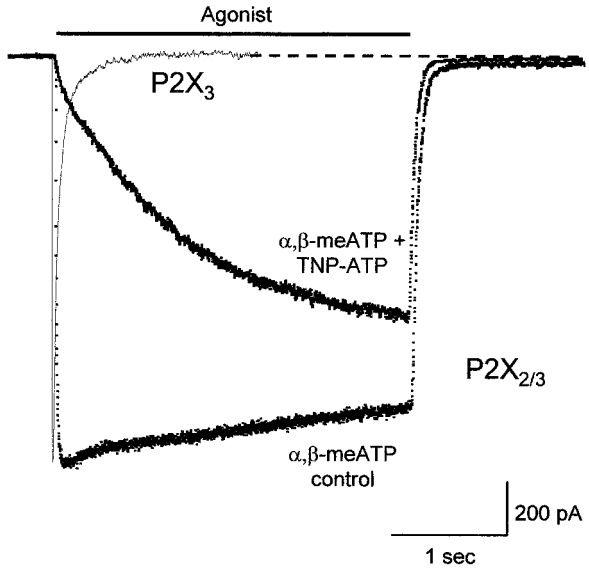

Fig. 7. Slow TNP-ATP kinetics can obscure competitive inhibition at $P2X_3$ receptors. Three superimposed traces recorded under different conditions. The light $P2X_3$ trace was recorded in response to 100 μM ATP. The dark $P2X_{2/3}$ responses were both recorded from a separate cell. α,β-meATP (100 μM, control) was either applied alone, or was applied in the presence of TNP-ATP (10 nM, TNP-ATP preapplication). Note the slow activation of $P2X_{2/3}$ receptors in the presence of TNP-ATP. Agonist application is denoted by the horizontal bar.

We propose a model (Fig. 7) to explain why TNP-ATP appears to be a noncompetitive antagonist at rapidly desensitizing $P2X_3$ receptors. When TNP-ATP is preapplied and allowed to reach equilibrium binding before an agonist is applied, agonist activation produces a $P2X_3$ response that desensitizes faster than TNP-ATP can dissociate from the receptor. Because $rP2X_3$ receptors desensitize with an initial rapid time course (τ = 39 ms; Burgard et al., 1999), desensitization will occur before a significant amount of TNP-ATP dissociates. In addition, the desensitization rate of $P2X_3$ receptors increases with increasing agonist concentration (Chen et al., 1995). Attempts to compete with TNP-ATP for receptor binding by increasing the agonist concentration can only make the agonist response faster, allowing even less time for antagonist dissociation. Under these conditions, competition with TNP-ATP will not be measured. However, competition can be measured at a relatively nondesensitizing receptor such as $P2X_{2/3}$.

The possibility that TNP-ATP can exhibit different antagonist actions (competitive versus noncompetitive) at different P2X receptors remains unlikely. $P2X_{2/3}$ receptors are formed by heteromultimeric combination of $P2X_3$ and $P2X_2$ subunits. Although the desensitization kinetics of $P2X_{2/3}$ receptors closely matches the $P2X_2$ phenotype, the pharmacology of the antagonist suramin, as well as that of agonists ATP and α,β-meATP, resembles that of $P2X_3$ receptors (Bianchi et al., 1999). The antagonist potency of TNP-ATP at $P2X_{2/3}$ receptors also matches that of $P2X_3$ receptors. Assuming that ATP, α,β-meATP, and TNP-ATP all bind at the same extracellular binding site on $P2X_{2/3}$ receptors, we would propose that this binding relationship is similar for $P2X_3$ receptors. TNP-ATP would therefore show competitive antagonism at both $P2X_3$ and $P2X_{2/3}$ receptors. Because of the rapid desensitization of $P2X_3$ receptors, this cannot be measured using standard electrophysiological techniques on wild-type receptors. The development of a sensitive and specific $P2X_3$ radioligand-binding assay could measure steady-state interactions between TNP-ATP and agonist, and could determine the competitive nature of TNP-ATP binding at $P2X_3$ receptors. The success of this approach would also depend on the ability of agonist to remain bound to the receptor after desensitization. Alternatively, this issue could be investigated electrophysiologically using a mutant $P2X_3$ receptor that retains $P2X_3$ binding properties, but has altered desensitization/gating kinetics. These approaches will require development of new tools for studying antagonist actions at P2X receptors.

Acknowledgments

We thank Karen Alexander, Heath McDonald, and Bruce Bianchi for assistance with experiments, and Lance Lee and Clark Briggs for valuable discussions.

References

Alkondon M, Pereira EF, Wonnacott S and Albuquerque EX (1992) Blockade of nicotinic currents in hippocampal neurons defines methyllycaconitine as a potent and specific receptor antagonist. *Mol Pharmacol* **41:**802–808.
Arunlakshana O and Schild HO (1959) Some quantitative uses of drug antagonists. *Br J Pharmacol* **14:**48–58.
Bean BP, Williams CA and Ceelen PW (1990) ATP-activated channels in rat and

bullfrog sensory neurons: Current-voltage relation and single-channel behavior. *J Neurosci* **10:**11–19.
Benveniste M and Mayer ML (1991) Kinetic analysis of antagonist action at *N*-methyl-D-aspartic acid receptors. *Biophys J* **59:**560–573.
Benveniste M, Mienville J-M, Sernagor E and Mayer ML (1990) Concentration-jump experiments with NMDA antagonists in mouse cultured hippocampal neurons. *J Neurophysiol* **63:**1373–1384.
Bianchi BR, Lynch KJ, Touma E, Niforatos W, Burgard EC, Alexander KM, Park HS, Yu H, Metzger R, Kowaluk EA, Jarvis MF and van Biesen T (1999) Pharmacological characterization of recombinant human and rat P2X receptor subtypes. *Eur J Pharmacol* **376:**127–138.
Briggs CA and McKenna DG (1996) Effect of MK-801 at the human alpha 7 nicotinic acetylcholine receptor. *Neuropharmacology* **35:**407–414.
Bultmann R, Wittenburg H, Pause B, Kurz G, Nickel P and Starke K (1996) P2-purinoceptor antagonists: III. Blockade of P2-purinoceptor subtypes and ecto-nucleotidases by compounds related to suramin. *Naunyn-Schmiedeberg's Arch Pharmacol* **354:**498–504.
Burgard EC, Niforatos W, van Biesen T, Lynch KJ, Touma E, Metzger RE, Kowaluk EA and Jarvis MF (1999) P2X receptor-mediated ionic currents in dorsal root ganglion neurons. *J Neurophysiol* **82:**1590–1598.
Chen CC, Akopian AN, Sivilotti L, Colquhoun D, Burnstock G and Wood JN (1995) A P2X purinoceptor expressed by a subset of sensory neurons. *Nature (Lond)* **377:**428–431.
Cheng Y and Prusoff WH (1973) Relationship between the inhibition constant (K1) and the concentration of inhibitor which causes 50 per cent inhibition (I50) of an enzymatic reaction. *Biochem Pharmacol* **22:**3099–3108.
Cloues R (1995) Properties of ATP-gated channels recorded from rat sympathetic neurons: Voltage dependence and regulation by Zn^{2+} ions. *J Neurophysiol* **73:**312–319.
Connolly GP (1995) Differentiation by pyridoxal 5-phosphate, PPADS and IsoPPADS between responses mediated by UTP and those evoked by alpha, beta-methylene-ATP on rat sympathetic ganglia. *Br J Pharmacol* **114:**727–731.
Craig DA (1993) The Cheng-Prusoff relationship: Something lost in the translation. *Trends Pharmacol Sci* **14:**89–91.
Ding S and Sachs F (1999) Single channel properties of P2X2 purinoceptors. *J Gen Physiol* **113:**695–720.
Evans RJ (1996) Single channel properties of ATP-gated cation channels (P2X receptors) heterologously expressed in Chinese hamster ovary cells. *Neurosci Lett* **212:**212–214.
Grubb BD and Evans RJ (1999) Characterization of cultured dorsal root ganglion neuron P2X receptors. *Eur J Neurosci* **11:**149–154.
Hiratsuka T and Uchida K (1973) Preparation and properties of 2′(or 3′)-O-(2,4,6-trinitrophenyl) adenosine 5′-triphosphate, an analog of adenosine triphosphate. *Biochim Biophys Acta* **320:**635–647.
Housley GD, Kanjhan R, Raybould NP, Greenwood D, Salih SG, Jarlebark L, Burton LD, Setz VC, Cannell MB, Soeller C, Christie DL, Usami S, Matsubara A, Yoshie H, Ryan AF and Thorne PR (1999) Expression of the P2X(2) receptor subunit of the ATP-gated ion channel in the cochlea: Implications for sound transduction and auditory neurotransmission. *J Neurosci* **19:**8377–8388.
Khakh BS, Bao XR, Labarca C and Lester HA (1999) Neuronal P2X transmitter-gated cation channels change their ion selectivity in seconds. *Nat Neurosci* **2:**322–330.
King BF, Wildman SS, Ziganshina LE, Pintor J and Burnstock G (1997) Effects of extracellular pH on agonism and antagonism at a recombinant $P2X_2$ receptor. *Br J Pharmacol* **121:**1445–1453.
Krishtal OA, Marchenko SM and Obukhov AG (1988) Cationic channels activated by extracellular ATP in rat sensory neurons. *Neuroscience* **27:**995–1000.
Lewis C, Neidhart S, Holy C, North RA, Buell G and Surprenant A (1995) Coexpression of P2X2 and P2X3 receptor subunits can account for ATP-gated currents in sensory neurons. *Nature (Lond)* **377:**432–435.
Lewis CJ, Surprenant A and Evans RJ (1998) 2′,3′-O-(2,4,6- Trinitrophenyl) adenosine 5′-triphosphate (TNP-ATP)—a nanomolar affinity antagonist at rat mesenteric artery P2X receptor ion channels. *Br J Pharmacol* **124:**1463–1466.
Lynch KJ, Touma E, Niforatos W, Kage KL, Burgard EC, van Biesen T, Kowaluk EA and Jarvis MF (1999) Molecular and functional characterization of human $P2X_2$ receptors. *Mol Pharmacol* **56:**1171–1181.
Mockett BG, Housley GD and Thorne PR (1994) Fluorescence imaging of extracellular purinergic receptor sites and putative ecto-ATPase sites on isolated cochlear hair cells. *J Neurosci* **14:**6992–7007.
Nicke A, Baumert HG, Rettinger J, Eichele A, Lambrecht G, Mutschler E and Schmalzing G (1998) P2X1 and P2X3 receptors form stable trimers: A novel structural motif of ligand-gated ion channels. *EMBO J* **17:**3016–3028.
Niforatos W, Burgard EC, Touma E, van Biesen T, Lynch KJ, Kowaluk EA and Jarvis MF (1999) Competitive antagonism of recombinant rat P2X receptors by TNP-ATP. *Soc Neurosci Abstr* **25:**171.
Ralevic V and Burnstock G (1998) Receptors for purines and pyrimidines. *Pharmacol Rev* **50:**413–492.
Stoop R, Thomas S, Rassendren F, Kawashima E, Buell G, Surprenant A and North RA (1999) Contribution of individual subunits to the multimeric P2X(2) receptor: Estimates based on methanethiosulfonate block at T336C. *Mol Pharmacol* **56:**973–981.
Thomas S, Virginio C, North RA and Surprenant A (1998) The antagonist trinitrophenyl-ATP reveals co-existence of distinct P2X receptor channels in rat nodose neurones. *J Physiol (Lond)* **509:**411–417.
Torres GE, Haines WR, Egan TM and Voigt MM (1998) Co-expression of P2X1 and P2X5 receptor subunits reveals a novel ATP-gated ion channel. *Mol Pharmacol* **54:**989–993.
Virginio C, Robertson G, Surprenant A and North RA (1998) Trinitrophenyl-substituted nucleotides are potent antagonists selective for P2X1, P2X3, and heteromeric P2X2/3 receptors. *Mol Pharmacol* **53:**969–973.
Watanabe T and Inesi G (1982) The use of 2′,3′-O-(2,4,6-trinitrophenyl) adenosine 5′-triphosphate for studies of nucleotide interaction with sarcoplasmic reticulum vesicles. *J Biol Chem* **257:**11510–11516.
Wright JM and Li C (1995) Zn^{2+} potentiates steady-state ATP activated currents in rat nodose ganglion neurons by increasing the burst duration of a 35 pS channel. *Neurosci Lett* **193:**177–180.
Zhong Y, Dunn PM and Burnstock G (2000) Guinea-pig sympathetic neurons express varying proportions of two distinct P2X receptors. *J Physiol (Lond)* **523:**391–402.

Send reprint requests to: Edward C. Burgard, Neurological and Urological Diseases Research, Department 4PM, Bldg. AP9A, Abbott Laboratories, Abbott Park, IL 60064-3500. E-mail: edward.c.burgard@abbott.com